Molecular Structure and Crystal Structure Generation for $[Fe_3(CO)_{12}]$†

Dario Braga,*[a] Fabrizia Grepioni,[a] Emilio Tedesco,[a] Maria José Calhorda*[b] and Pedro E. M. Lopes[b]

[a] *Dipartimento di Chimica G. Ciamician, Università di Bologna, Via Selmi 2, 40126 Bologna, Italy*
[b] *Instituto de Tecnologia Química e Biológica, R. da Quinta Grande 6, 2780 Oeiras, and Instituto Superior Técnico, Lisboa, Portugal*

The electronic structure of $[Fe_3(CO)_{12}]$ has been investigated by means of extended-Hückel calculations and compared to that of $[Ru_3(CO)_{12}]$, showing that the bridged structure, observed in the solid state, arises because of electronic reasons, namely a weaker metal–metal repulsion in the case of the lighter cluster. This is associated with the bridge-formation process and becomes determining for the energetic balance in compounds of heavier metals. The possible existence of crystal structures which are alternative to the observed disordered one known for $[Fe_3(CO)_{12}]$ has been explored by means of the atom–atom pairwise potential-energy method. Alternative ordered molecular arrangements have been generated and compared with the experimental crystal structure in terms of packing efficiency and cohesive energy.

The structure of $[Fe_3(CO)_{12}]$ has always attracted much attention in organometallic chemistry as witnessed by the large number of papers which have been published on various aspects.[1,2]

Recently, the solid-state molecular structure of $[Fe_3(CO)_{12}]$[3] has been reinvestigated by measuring X-ray diffraction data at different temperatures in the range 100–320 K.[4] It was shown that, as the temperature decreases, (*i*) the two bridging ligands, which span a single Fe–Fe bond, become progressively more symmetric leading to an almost exact C_{2v} molecular symmetry, and (*ii*) the bridged Fe–Fe bond length congruently decreases from 2.554(1) at 320 K to 2.540(2) Å at 100 K accompanying the bridging-ligand symmetrization whereas the two unbridged Fe–Fe bonds do not change appreciably.

This compound has also been subjected to a large number of theoretical studies based on different approaches, both semiempirical and *ab initio*,[5] and is one of the most intriguing of triangular M_3 clusters.[6] These theoretical studies, in turn, have complemented and originated many experiments aimed at understanding the fluxional behaviour of the carbonyl groups in solution.[7]

One of the interesting structural aspects of $[M_3(CO)_{12}]$ clusters, also found in other families of binary carbonyls, is the presence of two bridging carbonyls spanning the same Fe–Fe bond in the case of M = Fe. This side of the problem was addressed in general,[5d] while most of the other works dealt with the electronic structure and bonding inside the iron[5a,c] or ruthenium and osmium cluster.[5a,e] SINDO1 (symmetrically orthogonalized intermediate neglect of differential overlap) calculations[5b] have also recently been used to study the fluxionality problem and the interconversion between isomers of $[Fe_3(CO)_{12}]$. In molecular mechanics simulations[5i] the calculated bridged (C_{2v}) structure was in good agreement with the experimental structure. The importance of steric factors in determining the ligand distributions in $[M_3(CO)_{12}]$ complexes has also been addressed.[5g]

However, the fundamental question as to whether the bridged structure is a consequence of precise electronic requirements or whether steric factors contribute to or determine the actual structural choice with respect to the more homogeneous electronic distribution present in $[Ru_3(CO)_{12}]$[8] remains essentially unanswered. In this work, we shall try to address this question.

A second intriguing aspect of the structural problem of $[Fe_3(CO)_{12}]$ is related to the crystal structure, which, as mentioned above, is disordered. This disorder has been discussed in terms of either static or dynamic models. For instance, the results of ^{13}C cross polarization magic angle spinning (CP MAS) NMR experiments have been interpreted by assuming that the disorder arises from rotational jumps of the iron triangle within the CO-ligand shell.[9] This process is obviously temperature dependent so that only at 178 K the spectrum becomes consistent with the observed solid-state structure. In the 'static' view the disorder is instead believed to arise from the invariance to inversion of the quasi-icosahedral ligand shell around the Fe_3 triangle. Recent evidence obtained from a variable-temperature X-ray diffraction study[10] of the related species $[Fe_2Os(CO)_{12}]$ support the reorientational model (*i.e.* dynamic) of the disorder. The preferential orientation of the anisotropic displacement parameters of the iron atoms can also be accounted for by a large-amplitude librational motion of the Fe_3 triangle about the molecular two-fold axis.[11]

In order to address these problems we have investigated the electronic structure of $[Fe_3(CO)_{12}]$ and $[Ru_3(CO)_{12}]$ by means of theoretical calculations of the extended-Hückel type[12] and its crystal structure by generating alternative ordered crystals starting from the known molecular structure.[13] This latter possibility has been explored by examining first how two molecules can interact and interlock to form efficiently interlocked dimolecular nuclei (DMN) which can then be used to construct three-dimensional arrays. These procedures have been previously applied with success to study the molecular self-recognition and crystal-construction processes for neutral mono- and poly-nuclear complexes such as $[Co_2(CO)_8]$, $[Fe_2(CO)_9]$,[14a] $[Ni(CO)_4]$, $[Fe(CO)_5]$[14b] and $[Cr(CO)_6]$.[14c] In a similar manner, we have sought alternative ways to organize efficiently molecules of $[Fe_3(CO)_{12}]$ in crystal structures that are competitive with the experimentally observed one in terms of cohesion and volume occupation.

Similar combined approaches to molecular and crystal structure problems have been previously applied with success to

† *Non-SI units employed:* eV ≈ 1.60 × 10^{-19} J, cal = 4.184 J.

the understanding of the relationship between structural features and molecular organization in the solid for a number of other organometallic systems.[15]

Results and Discussion

Electronic Structure: Extended-Hückel Calculations.—The key structural difference between the $[M_3(CO)_{12}]$ clusters (M = Fe, Ru or Os) is the presence of two bridging carbonyls for the lighter element, in this case iron, spanning the same Fe–Fe bond, while the heavier clusters possess an all-terminal structure. Similar behaviour is observed in the family of $[M_4(CO)_{12}]$ clusters where only terminal carbonyls are present for M = Ir, whereas rhodium and cobalt clusters possess three bridging CO groups spanning a tetrahedron basal plane.[16] In this section, we describe our attempt to understand the difference between the two types of structures. The iron and the ruthenium clusters will be used as model structures and studied in greater detail.

The total energy is an indicator of how well the calculations reproduce the experimentally observed structures. Indeed, the energy of $[Fe_3(\mu\text{-}CO)_2(CO)_{10}]$ is lower by 0.75 eV than that of the all-terminal form, while $[Ru_3(CO)_{12}]$ is more stable than the corresponding bridged structure by 0.20 eV, in good agreement with experimental results. The structure having only terminal carbonyl groups is favoured for the heavier metal cluster. Bridges are seen in clusters containing a Ru_3 triangle only when a strong π-donor ligand is co-ordinated, as in $[Ru_3(CO)_9L]$ (L = trithiane) and discussed in a previous work.[15c]

Let us then analyse in more detail the iron cluster. The change in total energy and in the frontier orbitals for the conversion of one form into the other is shown in Fig. 1. The geometries are described in more detail in the Experimental section, but what happens is essentially the movement of two carbonyl groups (one from each of the two irons forming the metal–metal bond) from a terminal to a bridging position, while the other three terminal carbonyls rotate across one Fe–C bond, maintaining the geometry of the conical $Fe(CO)_3$ fragments (half octahedron) but modifying their relative positions, as depicted in Scheme 1.

This is similar to the mechanism put forward by Cotton[17] for the conversion between bridging and terminal carbonyls in solution, in which carbonyls move simultaneously ('the merry-go-round' process, model I, hereafter). This model is not exactly the 'merry-go-round' mechanism, but it is very close to it. On the other hand, we want to concentrate our attention on the two limiting structures, rather than on their interconversion for which we found an energy barrier of 26.5 kcal mol^{-1}. Two other mechanisms have been proposed: one based on the librational motion of the iron triangle about the molecular two-fold axis, and one based on rotation of the whole triangle about the metal cluster three-fold axis (models II and III, respectively). Both are based on the assumption that the Fe_3 triangle moves in the middle of the icosahedron defined by the carbon atoms of the carbonyl groups, which, in turn, is contained in an outer icosahedral polyhedron formed by the oxygens. The conversion of bridging into terminal structures can be achieved by rotation of the triangle around the two-fold axis in the icosahedron (model II), or by 60° rotational jumps around the pseudo-three-fold one (model III). In the more elaborate forms of these models the outer atoms are allowed to relax, instead of remaining fixed throughout the movement. Comparison of the three mechanisms has been addressed theoretically by SINDO1 calculations[5b] and the energy barriers were estimated to be 14 kcal mol^{-1}, for model I, >43 kcal mol^{-1} for II and 150 kcal mol^{-1} for III, in comparison to the 10 kcal mol^{-1} experimental value obtained in the solid state by ^{13}C CP MAS NMR spectroscopy. The first model seems the most likely possibility and our higher value is not surprising, considering the absence of geometry optimizations. Molecular-mechanics calculations

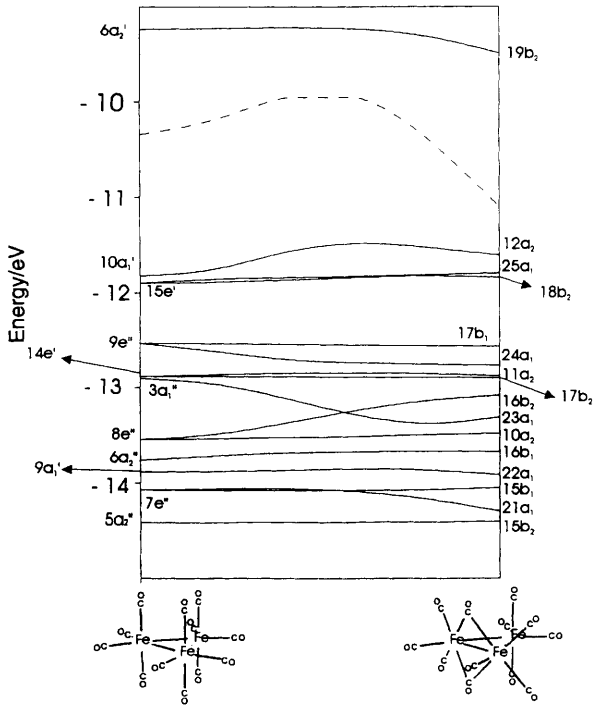

Fig. 1 Change in total energy (– – –) and in frontier orbitals for conversion of the terminal structure of $[Fe_3(CO)_{12}]$ into the bridging one

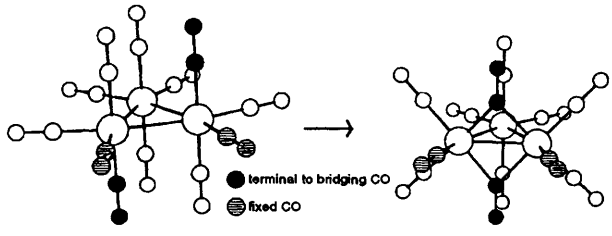

Scheme 1

are in agreement with both models II and III,[18] which are also supported by the experimental evidence on $[Fe_2Os(CO)_{12}]$.[10]

In order to understand why one geometry is favoured for the iron cluster the Walsh diagram in Fig. 1 should be analysed. Though the terminal structure has D_{3h} symmetry and the bridging one C_{2v}, the only symmetry kept along the conversion path is C_2. The labels correspond to D_{3h} and C_{2v} symmetry. There is not an obvious orbital which can be assigned as responsible for the trend, though $9e'' \longrightarrow 24a_1$ and $3a_1'' \longrightarrow 23a_1$ are strong candidates. They become more stable after the conversion. The $3a_1'' \longrightarrow 23a_1$ orbital, for example, is stabilized because it starts as almost Fe–C non-bonding and Fe–Fe antibonding (δ*) and ends as Fe–C bonding and Fe–Fe σ bonding in the bridged structure as shown in Fig. 2.

We should keep in mind that the formation of the two bridges is accompanied by the rotation of the $Fe(CO)_3$ groups. As a consequence, the relative orientation of $Fe(CO)_3$ groups and, therefore, the frontier orbitals of the $Fe_3(CO)_{10}$ fragment interacting with two carbonyls (either terminal or bridging) is modified. In order to understand the behaviour of the Walsh orbitals, we need to understand, first, what the differences introduced by the rotation are, and then the different way two terminal, or two bridging, carbonyls interact with them. The easiest way is to start from the well known $Fe(CO)_3$ fragment, which is a half octahedron and has well described frontier orbitals.[19] From them we can build two dimers, **a** and **b** in Scheme 2, differing by their relative orientation. A similar dimer formation has been studied, as well as the problem of adding

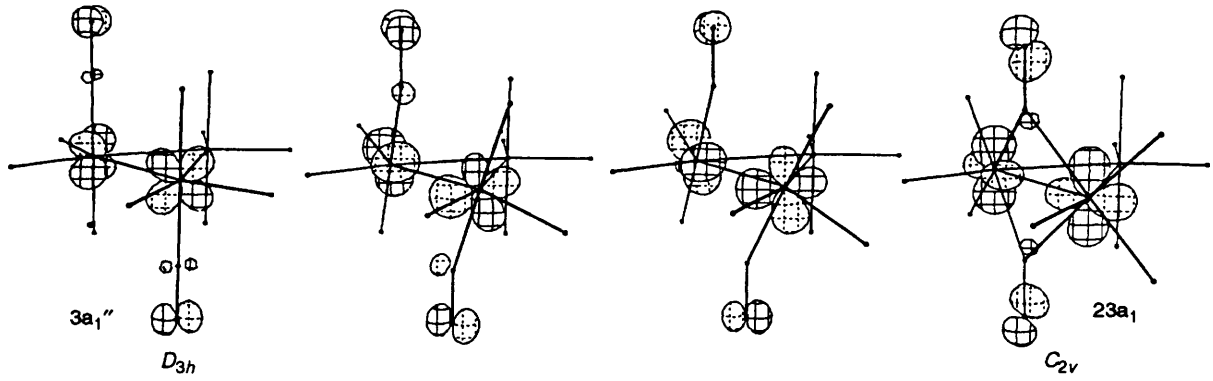

Fig. 2 The change along the conversion for the $3a_1'' \longrightarrow 23a_1$ orbital shown in Fig. 1

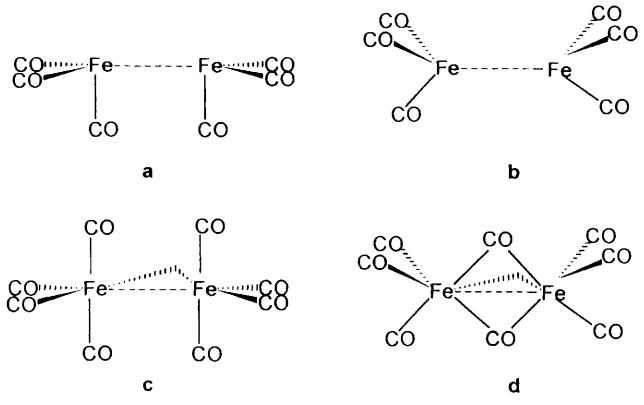

Scheme 2

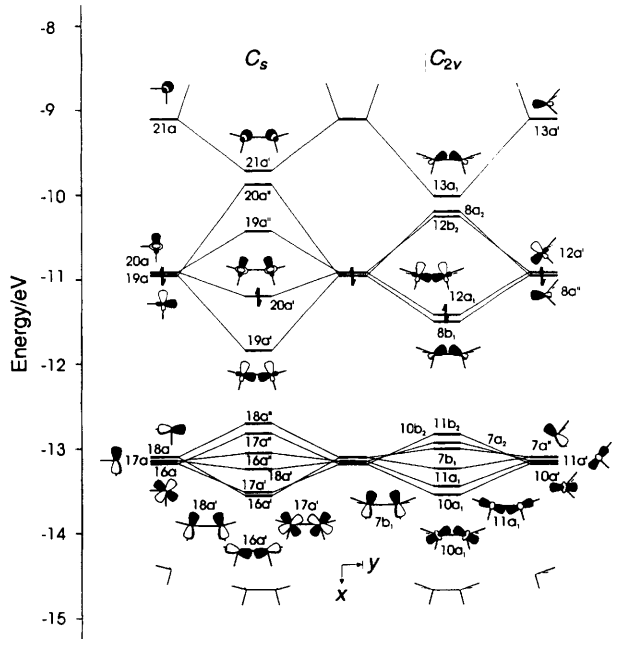

Fig. 3 Interaction between two $Fe(CO)_3$ groups in two different relative orientations to give the fragments **a** (left) and **b** (right)

terminal and bridged carbonyls.[20] The process is shown in Fig. 3. The remaining vertex of the triangle, $Fe(CO)_4$, will be added to give the final fragments which will interact with two carbonyl groups, either terminal, **c**, or bridging, **d** [the $Fe(CO)_4$ vertex is not shown]. The frontier orbitals of this d^8 ML_4 fragment have also been described before.[19]

The pyramidal $Fe(CO)_3$ retains the frontier d orbitals of the octahedron geometry, namely one t_{2g}-like set of low energy, followed by the two e_g-type orbitals. At slightly higher energies there is another important empty orbital, which has mixed s and p character.[17] Their energies are shown both in the centre and in the outer sides of Fig. 3.

The two fragments approach each other as represented in **a** and **b** and they mainly interact through the 'e_g' orbitals, better directionalized than the t_{2g} ones, giving rise to a metal–metal bond having double-bond character. The high-energy hybrids (21a or 13a') overlap, but the molecular orbitals are empty. On the other hand, all t_{2g} orbitals are involved in destabilizing four-electron interactions. The global overlap is comparable for the two structures (0.45 for C_s, 0.46 for C_{2v}), though two bonding molecular orbitals (MOs) of similar energy are obtained for the species of C_{2v} symmetry, while for the C_s moiety one orbital is much more stabilized than the other. The fragment leading to the bridged isomer of $[Fe_3(CO)_{12}]$ (**b**, C_{2v}) is only slightly more stable at this stage.

We now continue, adding the other vertex of the triangle, the $Fe(CO)_4$ unit. In the centre of Fig. 4 are represented the orbitals of the two $Fe_2(CO)_6$ fragments (**a** and **b**) previously built (Fig. 3). They interact with the orbitals of $Fe(CO)_4$, typical of a d^8 ML_4 fragment,[19] which occupy the outer parts of the figure. The main skeleton of the final clusters (**c** and **d**, without the two last CO groups) is formed.

The principal interactions involve the two 'e_g' orbitals of $Fe(CO)_4$, one empty, another occupied, as the other four-electron destabilizing interactions do not differ too much for the two forms. In a simplified way, the two new Fe–Fe bonds can be described by donation of electrons from 9a″ or $6b_2$ to the binuclear fragments (19a″, 20a″ $12b_2$) and back donation into empty 16a' or $10a_1$. The resulting bonding molecular orbitals are not significantly different for the two situations, but the second-highest-occupied MO of $Fe_2(CO)_6$ ($8b_1$) is much more destabilized by the repulsive interaction with the $6b_1(t_{2g})$ orbital of $Fe(CO)_4$ for the bridged geometry, and to such an extent that the 'terminal' trinuclear fragment becomes more stable. The bridged species has a higher energy highest-occupied molecular orbital (HOMO).

Only addition of the two final carbonyls remains. The interactions taking place when forming **c** and **d** are shown in Fig. 5, and are those expected from carbonyls, with both donation and back-donation components.

The interesting part, again responsible for stabilizing the bridged geometry, is that two empty orbitals ($11a_2$ and $2a_2$) interact strongly, so that the resulting bonding molecular orbital takes the two electrons which previously occupied the high-energy HOMO of the metallic fragment (35a' or $21a_1$). This interaction involves the π orbitals of the carbonyl ligands and therefore is considered as one of the back-donation components, as if initially two electrons occupied 35a' and $14b_1$ rather than 34a' and $21a_1$. This molecular orbital is Fe–C bonding, but strongly Fe–Fe antibonding. On the whole, the strongest interaction taking place is that involving the bridging

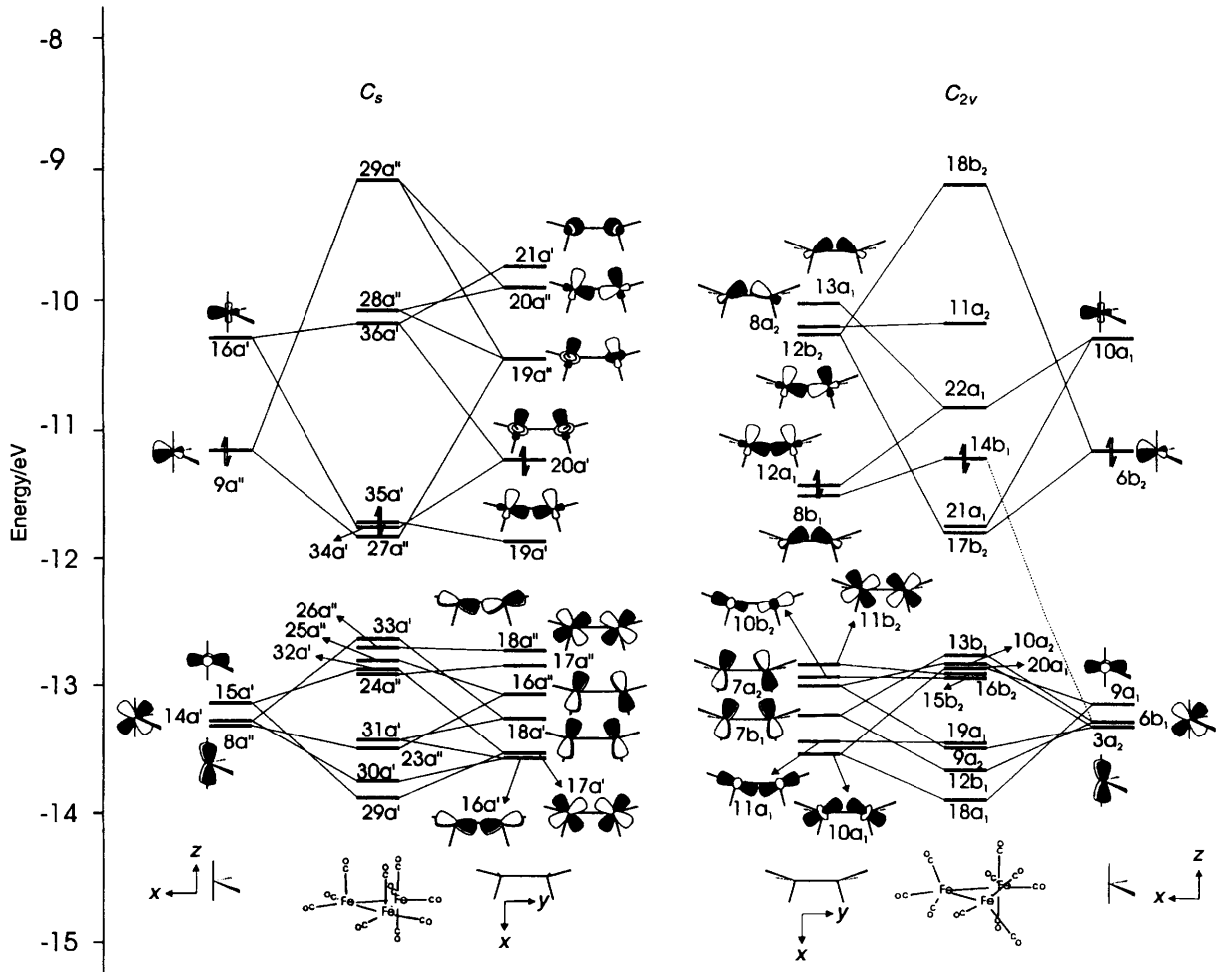

Fig. 4 Interaction between two $Fe_2(CO)_6$ fragments of C_s (left) and C_{2v} (right) symmetry with $Fe(CO)_4$

Table 1 Relative energies (eV) and overlap populations between fragments (in parentheses) for the steps involved in cluster building

Species	Iron	Ruthenium
$M(CO)_3$ + $M(CO)_3$ bridged	0 (0.046)	0.30 (0.034)
$M(CO)_3$ + $M(CO)_3$ terminal	0.17 (0.046)	0 (0.039)
$M_2(CO)_6$ + $M(CO)_4$ bridged	0.18 (0.055)	0.54 (0.056)
$M_2(CO)_6$ + $M(CO)_4$ terminal	0 (0.063)	0 (0.063)
$M_3(CO)_{10}$ + $(CO)_2$ bridged	0 (0.202)	0.21 (0.155)
$M_3(CO)_{10}$ + $(CO)_2$ terminal	0.25 (0.172)	0 (0.178)

carbonyls (overlap population between fragments 0.202, compared to 0.172 for the terminal geometry). We can trace the main factor responsible for the greater stabilization of the structure with the bridges: two bridging carbonyls interact more strongly than two terminal ones with the preformed $Fe_3(CO)_{10}$ fragments.

Having these results in mind, let us now examine the ruthenium clusters. In Table 1 are reported the energies and overlap populations between fragments obtained when constructing the iron and ruthenium clusters following the above procedure (the 0 value indicates for each case the most stable form; the energies are relative).

In the first step, ruthenium favours the terminal structure. The two occupied molecular orbitals resulting from interaction between two $Ru(CO)_3$ fragments are more stable for the terminal form (compare with Fig. 3 for the iron case). When the third metal in the triangle is added the interaction is always better for the terminal than the bridged form and the stability of the two forms is reversed for iron (see Fig. 4 for iron). Addition of bridging carbonyls led to a great stabilization in iron clusters, as described above (Fig. 5), but it does not have the same effect for ruthenium. The HOMO of the cluster, as for $[Fe_3(CO)_{12}]$, is derived from a similar interaction between empty orbitals of the fragments. The bonding component, metal–metal antibonding and M–C bonding, is again stabilized. It is not so much stabilized for ruthenium, however, as it was for iron, as repulsion between the metals is stronger in this case. This effect is detected both in the $Ru_3(CO)_{10}$ fragment, where the orbital has a relatively higher energy than the comparable orbital in the iron system, and also in the final cluster. As a consequence of the lack of stabilization introduced by this interaction, the bridged structure has a higher energy and the terminal structure prevails.

As hinted by previous workers,[5d] the formation of carbonyl bridges is favoured by first-row metals, as the metal–metal antibonding character introduced in metal–carbon bonding orbitals (resulting from back donation) is weak enough to be allowed. Moving to heavier metal derivatives, this factor becomes more and more important, though the final balance depends also on other ligands of the cluster.[14c]

Crystal Structure Decoding and Generation.—After having examined the molecular structure of $[Fe_3(CO)_{12}]$ we can now attempt to understand whether this molecule can be organized in the solid state in structures which are alternative to the observed disordered one. We have discussed on several previous

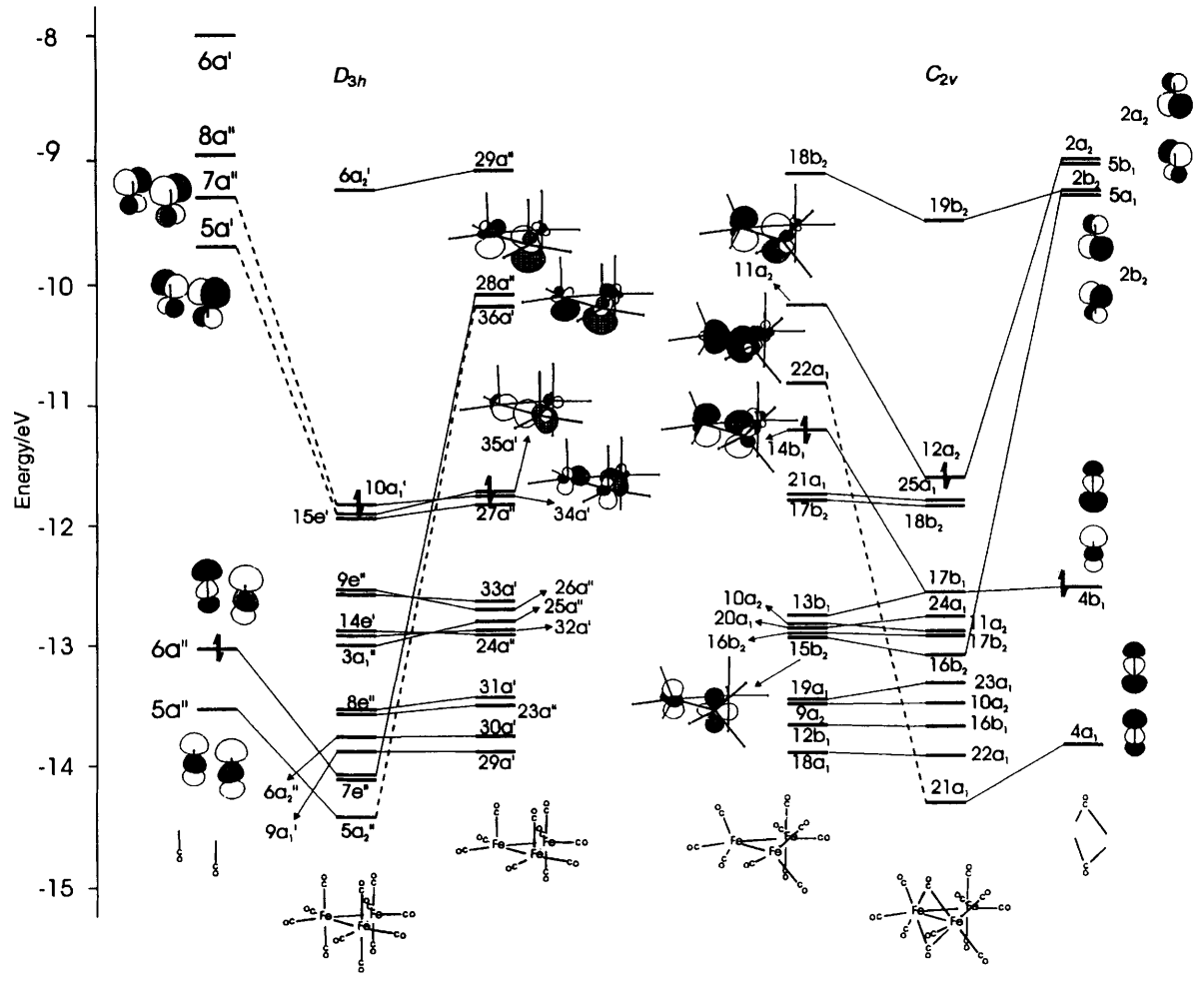

Fig. 5 Interaction between two terminal and two bridging carbonyls with $Fe_3(CO)_{10}$ fragments of symmetry C_s and C_{2v}, to form $[Fe_3(CO)_{12}]$ with the terminal structure (**c**, left) and the bridging one (**d**, right)

occasions[21] how the crystal structures of neutral transition-metal clusters obey essentially the same rules of close packing as those of organic molecules. The molecular arrangement in such crystals can easily be decoded by studying the number, distribution, and pattern of intermolecular interactions between a reference molecule in the crystal and the surrounding molecules. This approach has been applied, for example, to decoding of the crystal structure of $[Ru_3(CO)_{12}]$.[22]

As mentioned above the crystal structure of $[Fe_3(CO)_{12}]$ is disordered: a crystallographic centre of inversion relates the two alternative orientations of the metal triangle as well as those of the carbonyl ligands. These two orientations are thus present with equal occupancy in the average crystal structure in the space group $P2_1/n$ observed in the diffraction experiment. A limiting ordered molecular distribution can be described as a monoclinic $P2_1$ crystal if the centre of inversion is ideally 'removed' from the experimental crystal structure. The resulting unit cell contains two molecules related only by the screw axis as shown in Fig. 6.

We now know that the molecular structure of $[Fe_3(CO)_{12}]$ observed in the solid state corresponds to the most stable structure of the isolated (ideally gas-phase) molecule. Hence, we can use the molecular structure present in the experimental crystal structure to attempt generation of alternative three-dimensional molecular organizations, *viz.* of new crystal structures. The procedure and methods used for crystal-structure generation have been discussed extensively in previous publications by some of us and by Gavezzotti. The reader is addressed to these earlier papers for details.[13,14] Here we need only summarize the essential steps.

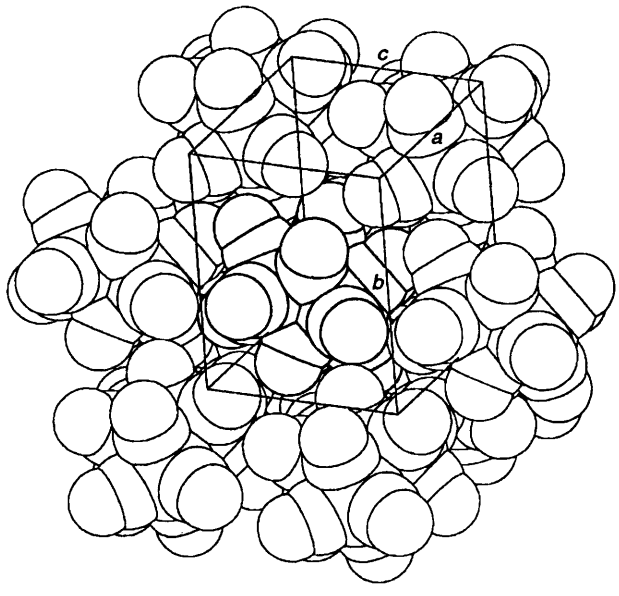

Fig. 6 The ideally ordered monoclinic $P2_1$ crystal obtained from the experimental structure of $[Fe_3(CO)_{12}]$ by 'removing' the centre of inversion

(*i*) *Choice of potential parameters.* Parameters to be used in the subsequent calculations are first checked against the experimental structure. The effect of the various sets of potential parameters is investigated by performing structure refinement ('annealing') on the experimental structure with the crystal and site symmetry preserved. The working hypothesis is that the best parametrization is that causing the minimum changes to the experimental structure. In the present study the potential parameters adopted for carbon and oxygen are the 'generalized' parameters put forward by Gavezzotti and Filippini,[23] while the Fe atoms are treated as the corresponding noble gas, krypton.

(*ii*) *Generation of dimolecular nuclei (DMN).* Nuclei formed by two molecular units are generated by searching the space surrounding a reference molecule for optimum location of symmetry operators such as the inversion centre (**I**) and the screw axis (**S**). The effect of translational symmetry (**T**) is also explored at this stage. The intermolecular energy of the DMN (dimer energy, E_D/kcal mol^{-1}) is calculated and compared with the cohesive energy of the DMN present in the experimental structure.

(*iii*) *Generation of new crystal structures.* Once a DMN has been selected on the basis of its E_D, the translational search and subsequent crystal-structure optimization can be performed leading to the final calculated crystal structure. Crystal structures can be generated in all most common space groups ($P\bar{1}$, $P2_1$, $P2_1/c$, $P2_12_12_1$),[14b] depending on the reciprocal combination of symmetry operators and of these with the translational search. The calculated crystal structures are then compared in terms of cohesive energy (E_C) and of efficiency of space occupation, with the experimental structure.

As mentioned above, this procedure has been successfully tested in a number of cases. The disorder in crystalline $[Fe_3(CO)_{12}]$, however, poses an additional problem because crystal-structure refinement cannot be carried out on a disordered crystal in which the molecules can randomly adopt two different orientations. We can only check the performance of the potential parameters on the limiting $P2_1$ structure formed by ordered molecular arrays, assuming that this structure represents the behaviour of the experimental structure under the action of the potential parameters. Moreover, a rigid molecular structure has to be assumed. This is only partially correct in the case of $[Fe_3(CO)_{12}]$ because its structure is affected by the temperature. There is no way around this problem. Therefore we have performed all following calculations starting from the room-temperature data set because the carbon and oxygen atom potential parameters we use for crystal-structure generation are optimized on crystal structures determined at room temperature.

The effect of crystal-structure refinement is shown in Table 2. It can be seen that, when the generalized potential parameters are used, the difference is confined to the *a* axis, which contracts slightly whereas the other two axes and the monoclinic angle barely change. In terms of the efficiency of packing and of packing potential energy values the two cells are practically identical. As mentioned above, this can be taken as indicative that the generalized potential parameters are adequate for describing the observed molecular interactions in $[Fe_3(CO)_{12}]$ as in many other binary carbonyls of first-row metals.

The two DMN with greatest cohesion present in crystalline $[Fe_3(CO)_{12}]$ are shown in Fig. 7(*a*) and 7(*b*). These DMN are generated by the screw axis and by the combined screw-inversion operations which relate the two images in the disordered crystal structure. The most cohesive DMN are listed in Table 3. The DMN are compared with the observed ones in terms of dimer cohesive energy (E_D) and of intermolecular separation (the distance between the centres of mass). The DMN obtained in the **I** and **S** search (structures Fe_3-**I** and Fe_3-**S**) will now be described. The DMN obtained *via* pure translation (structure Fe_3-**T**) will also be discussed.

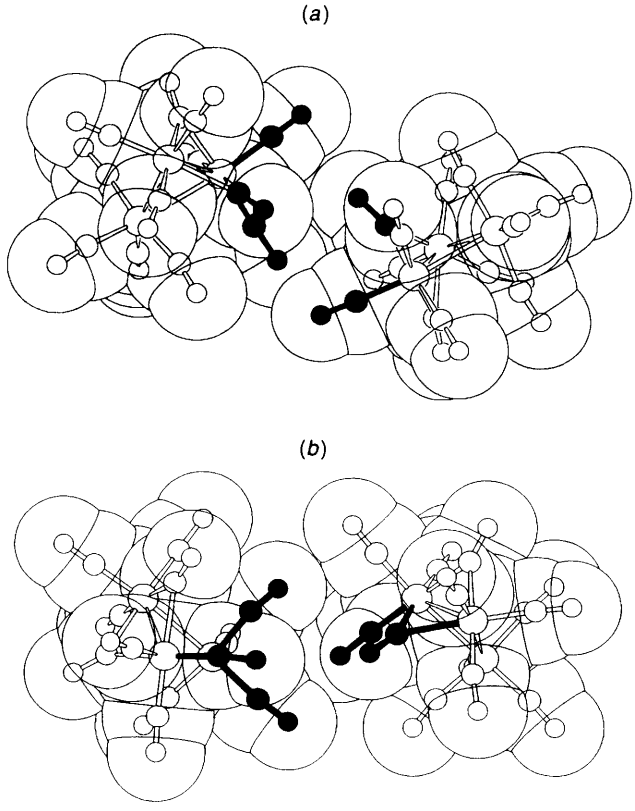

Fig. 7 The two most cohesive DMN present in crystalline $[Fe_3(CO)_{12}]$: (*a*) generated by the screw axis, (*b*) generated by a combined screw-inversion operation

Table 2 Structural relaxation of the experimental crystal structure

Parameter	Exptl.*	Relaxed
a/Å	8.359	8.368
b/Å	11.309	11.309
c/Å	8.862	8.862
α/°	90.00	90.00
β/°	97.00	97.04
γ/°	90.00	90.00
p.c.	0.67	0.66
p.p.e./kcal mol^{-1}	−62.1	−62.1

* Limiting ordered $P2_1$ structure.

Table 3 Comparison between calculated and observed DMN

DMN	Symmetry operator(s)*	Intermolecular separation/Å	E_D/kcal mol^{-1}
Fe_3-obs	**S**	7.980	−5.9
	T	8.098	−5.2
Fe_3-**T**	**T**	8.084	−6.6
Fe_3-**I**	**I**	8.080	−7.3
Fe_3-**S**	**S**	8.060	−7.0
Fe_3-**S-I**	**S** + **I**	8.134	−6.2
Fe_3-**S-S**	**S** + **S**	8.134	−5.1

* **S** = screw, **T** = translation, **I** = inversion.

The **T**-DMN in structure Fe_3-**T** is highly competitive with the observed ones (E_D = −6.6 kcal mol^{-1}). The interlocking is shown in Fig. 8(*a*). It can be seen that the two equatorial CO groups of the $Fe(CO)_4$ unit embrace one bridging CO of the next neighbour, while a tricarbonyl unit formed by two radial and one axial CO in one molecule interacts with a $(CO)_3$ unit formed by one bridging and two radial CO in the second molecule. More interesting is the DMN obtained *via* inversion

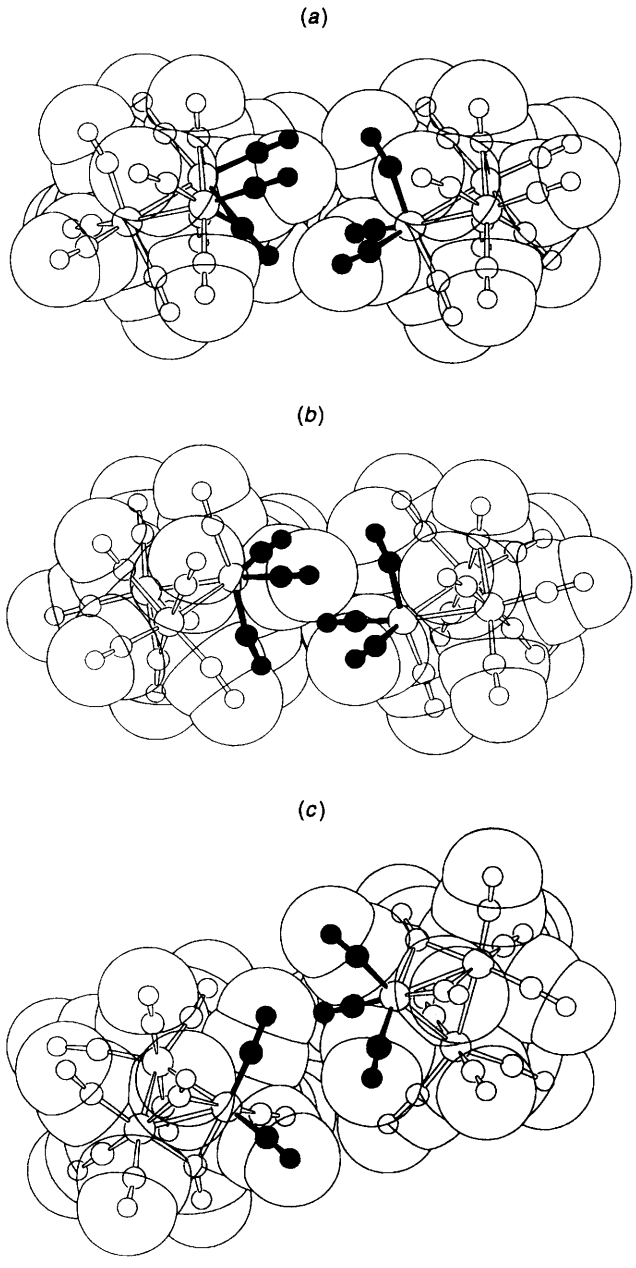

Fig. 8 (*a*) Calculated **T**-DMN (structure Fe_3-**T**, $E_D = -6.6$ kcal mol^{-1}) where two equatorial CO of the $Fe(CO)_4$ unit embrace one bridging CO of the next neighbour. (*b*) The DMN obtained *via* inversion ($E_D = -7.3$ kcal mol^{-1}). (*c*) The **S**-DMN based on $(CO)_3 \cdots (CO)_3$ interlocking

in structure Fe_3-**I**. As in the case of the **T**-DMN, the two molecules are interlocked *via* interaction of the type $(CO)_3 \cdots (CO)_3$ between the tricarbonyl units belonging to the Fe atom carrying only terminal ligands [see Fig. 8(*b*)]. This DMN appears to be, by far, the most cohesive ($E_D = -7.3$ kcal mol^{-1}) and one may wonder why it has not been adopted in the construction of the crystalline material.

The search procedure generated three different **S**-DMN in the three crystals in $P2_1$, $P2_1/c$, $P2_12_12_1$ symmetry (structures Fe_3-**S**, Fe_3-**S-I** and Fe_3-**S-S**, respectively). The most cohesive **S**-DMN is obtained in the $P2_1$ structure (Fe_3-**S**) and shows the same interlocking motif as the **T**- and **I**-DMN, *i.e.* $(CO)_3 \cdots (CO)_3$ interlocking. Hence, tricarbonyl units interlocked along their three-fold axes play a fundamental role in the packing of metal carbonyls. The E_D values for the three DMN are very similar as shown in Table 3. The most cohesive **S**-DMN belonging to structure Fe_3-**S-I** is shown in Fig. 8(*c*).

These calculated DMN can now be translated in the three directions of space in order to obtain a crystal structure. The calculated structures will be compared in terms of packing coefficient (p.c.) and cohesive energy (E_C) with the experimental structure in its limiting representation. The results of the crystal-generation procedure are listed in Table 4. The p.c. has been estimated according to the formula $V_{mol}Z/V_{cell}$ where V_{mol} is calculated with the integration method put forward by Gavezzotti.[24] The molecular volume is obtained by sampling the space occupied by the molecule by summing up the occurrences of a unit volume falling within the van der Waals sphere of any one atom in the molecule. It can be anticipated that, contrary to what is observed in the cases of $[Co_2(CO)_8]$ and $[Fe_2(CO)_9]$, the theoretical structures for $[Fe_3(CO)_{12}]$ are all slightly less cohesive than is the experimental one. Nonetheless, the procedure succeeded in producing valid alternatives to the molecular organization of this molecule which, for the most representative cases, are worth a more detailed examination.

The two triclinic crystals ($P1$ with $Z = 1$ and $P\bar{1}$ with $Z = 2$) can be discussed together. The two crystals are not competitive with experimental structure (p.c. 0.62 and 0.65; $E_C = -54.05$ and -58.19 kcal mol^{-1}, respectively). Fig. 9(*a*) shows the molecular arrangement for the $P\bar{1}$ structure which is constructed around the **I**-DMN discussed above. It would appear that, although pure translation along one direction leads to good one-dimensional packing, packing cohesion is lost when the preformed molecular rows are put side by side to form layers and then the final three-dimensional crystal structure. The calculated Fe_3-**I** structure possesses a cell volume larger than that of the experimental structure (857.4 *vs.* 831.5 $Å^3$).

Structures Fe_3-**S** and Fe_3-**S-I** obtained in space groups $P2_1$ and $P2_1/c$ respectively are both *ca.* 5% less dense than the experimental structure. It is worth noting that in the latter crystal the *c* value is almost double the *a* value in the former.

Table 4 Calculated crystal structures for $[Fe_3(CO)_{12}]$*

Code	Space group	p.p.e./kcal mol^{-1}	p.c.	*a*/Å	*b*/Å	*c*/Å	α/°	β/°	γ/°	*U*/$Å^3$
Fe_3-obs	$P2_1/n$	−62.1	0.67	8.359	11.309	8.862	90.0	97.0	90.0	831.5
Fe_3-**T**	$P1$	−54.1	0.62	8.084	8.818	9.656	53.37	53.80	66.20	444.4
				(8.330)	(8.818)	(8.084)	(113.8)	(104.9)	(111.5)	(444.4)
Fe_3-**I**	$P\bar{1}$	−58.2	0.65	9.403	9.322	9.809	85.88	90.14	88.92	857.4
				(9.403)	(9.809)	(9.322)	(94.12)	(91.08)	(90.14)	(857.4)
Fe_3-**S**	$P2_1$	−53.6	0.63	9.798	9.806	9.226	90.0	93.58	90.0	884.7
				(9.226)	(9.806)	(9.798)	(90.0)	(93.58)	(90.0)	(884.7)
Fe_3-**S-I**	$P2_1/c$	−48.6	0.59	8.019	15.586	16.257	90.0	66.54	90.0	1863.9
				(8.019)	(15.586)	(14.993)	(90.0)	(95.92)	(90.0)	(1863.9)
Fe_3-**S-S**	$P2_12_12_1$	−55.8	0.63	11.872	8.634	17.051	90.0	90.0	90.0	1747.8
				(11.872)	(17.051)	(8.634)	(90.0)	(90.0)	(90.0)	(1747.8)

* Values for Niggli reduced cells and alternative unit-cell settings are in the parentheses.

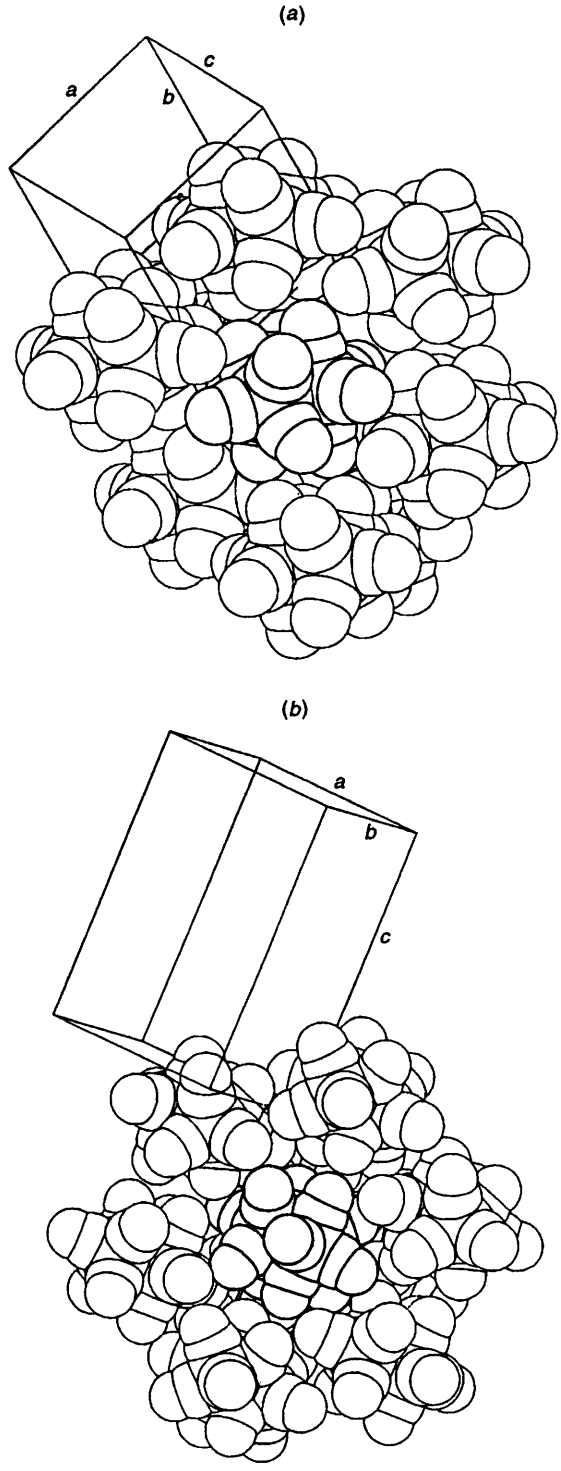

Fig. 9 Intermolecular interlocking and molecular arrangement in (*a*) structure Fe_3-I (space group $P\bar{1}$) and (*b*) structure Fe_3-S-S (space group $P2_12_12_1$)

The solution obtained in the orthorhombic space group $P2_12_12_1$ (structure Fe_3-S-S) shows the same packing coefficient as that of the monoclinic $P2_1$ solution (p.c. = 0.63). The intermolecular interlocking, in its space-filling representation, is shown in Fig. 9(*b*).

Conclusion

We have tackled two distinct, though strictly related, problems concerning $[Fe_3(CO)_{12}]$, namely that of its molecular structure and that of its crystal structure. Molecular and crystal structures for flexible organometallic molecules are intimately interconnected. Both factors have precise influence on the minimization of the global energy of the system formed by the molecules packed in the solid state. These free-energy minima, however, are seldom unique. The number of possible isoenergetic solutions increases as the energy difference between structural forms for the isolated molecules (isomers) are within the differences in cohesive energy that can be obtained in crystals.

The problem of whether the molecular structure of $[Fe_3(CO)_{12}]$ corresponds to that of the (hypothetical) isolated molecule as well as the different distribution and bonding modes of the CO ligands in $[Fe_3(CO)_{12}]$ and $[Ru_3(CO)_{12}]$ has been addressed by extended-Hückel calculations. The results can be summarized as follows: the formation of structures containing bridging carbonyls is, in principle, favoured owing to the greater number of bonds in the molecule. However, bridge formation implies occupation of previously empty, high-energy orbitals with metal–metal antibonding character which are pushed down by interaction with π^* orbitals of the bridging carbonyls. This repulsive metal–metal interaction may distort the balance between bridged or non-bridged structures toward the last, when the metal d orbitals are less contracted and thus this term becomes more important.

We have also tried to generate alternative ordered crystal structures for $[Fe_3(CO)_{12}]$. Since this molecule possesses a pseudo-icosahedral shape, the results could be (at least in principle) transferred to other cluster systems possessing the same peripheral polyhedron of ligands such as, for instance, $[Co_4(CO)_{12}]$, $[Rh_4(CO)_{12}]$, and their derivatives, as well as to most derivatives of $[Ir_4(CO)_{12}]$. We have succeeded in obtaining a number of ordered packing arrangements which differ by a few kcal mol^{-1} from the experimental structure. We are unable, however, to evaluate the entropy contribution to the formation of one or the other crystal structure, nor can we take into account the formation of a disordered system. Furthermore, having shown that $[Fe_3(CO)_{12}]$ has a molecular structure which is the lowest-energy structure for the isolated molecule and that this structure is preserved in the solid state with its near-icosahedral, and therefore near-centrosymmetric, ligand polyhedron, it is clear that the potential-energy hypersurface around the molecule is rather shallow and allows the approach of molecules in several ways. We have been able to recognize the most relevant interlocking motif, namely the interlocking between tricarbonyl units, which is present in all calculated structures and, therefore, we have gained insights into the molecular recognition process which leads to nucleation and crystal formation.

It is worth stressing, that there is much current interest in procedures and methods which could help understand the factors controlling crystal nucleation and molecular aggregation. The engineering of new materials with predefined physical and/or chemical properties would be greatly advanced by even the smallest step in this direction.[25]

Experimental

All the molecular orbital calculations were done using the extended-Hückel method[12] with modified H_{ij} values.[26] The basis set for the metal atom consisted of *n*s, *n*p and (*n* − 1)d orbitals. The s and p orbitals were described by single Slater-type wavefunctions, and the d orbitals were taken as contracted linear combinations of two Slater-type wavefunctions. Standard parameters were used for H, C, O and S, while those for Fe and Ru are reported in Table 5. The program CACAO was used for calculations and for drawing three-dimensional representations of orbitals.[27]

Idealized models for $[M_3(CO)_{12}]$ (M = Fe or Ru) having C_{2v} and D_{3h} symmetry were used for the clusters studied, based on the geometries of the observed clusters.[3,8] The following

Table 5 Parameters for Slater-type wavefunctions for iron and ruthenium atomic orbitals

Atom	Parameter	Orbital		
		*n*s	*n*p	$(n-1)$d
Fe ($n = 4$)	ζ/ζ_1	1.900	1.900	5.350
	ζ_2			1.800
	H_{ij}/eV	−9.170	−5.370	−12.700
	c_1			0.5366
	c_2			0.6678
Ru ($n = 5$)	ζ/ζ_1	2.078	−10.400	5.378
	ζ_2			2.303
	H_{ij}/eV	2.043	−6.890	−14.900
	c_1			0.5340
	c_2			0.6365

Table 6 Parameters for the packing potential energy calculations in the form p.p.e. = $Ae^{-Br} - Cr^{-6}$/kcal mol^{-1} (r in Å)

Interaction*	A/kcal mol^{-1}	B/Å^{-1}	C/Å^6 kcalmol^{-1}
Fe · · · Fe as Kr · · · Kr	270 600	3.28	3 628
C · · · C	54 050	3.47	578
O · · · O	46 680	3.74	319
C · · · O	93 950	3.74	641

* Cross-interactions (Fe · · · C, Fe · · · O) from $A_{xy} = (A_{xx}A_{yy})^{\frac{1}{2}}$, $B_{xy} = \frac{1}{2}(B_{xx} + B_{yy})$, $C_{xy} = (C_{xx}C_{yy})^{\frac{1}{2}}$.[29]

distances (Å) were used: Ru–Ru 2.85, Ru–C(terminal) 1.896, Ru–C(bridging) 2.086, C–O 1.13, Fe–Fe 2.600, Fe–C(terminal) 1.82, Fe–C(bridging) 1.973. The conical $Fe(CO)_3$ fragment was taken as a half octahedron.

The packing potential energy (p.p.e.) of an organometallic molecule can be estimated by applying empirical methods similar to those usually employed in the neighbouring field of solid-state organic chemistry. Use is made of the expression p.p.e. = $\Sigma_i\Sigma_j[A \exp(-Br_{ij}) - Cr_{ij}^{-6}]$, where r_{ij} is the non-bonded atom–atom intermolecular distance. Index i in the summation runs over all atoms of the reference molecule and j over the atoms of the surrounding molecules.[28] In previous studies we discussed the effects of using the generalized potential parameters obtained by Gavezzotti and Filippini.[23] These parameters were compared with other available sets. The parameters used to obtain the energies reported in Tables 2–4 are shown in Table 6. A slightly modified version of the computer program OPEC was used for all calculations of packing potential energies and to estimate packing coefficients and intermolecular interactions.[24] The refinement of the observed structure was performed by using PCK 83[30] which allows an optimization of the packing energies with respect to the cell parameters and molecular rigid-body translation and rotation. Dimolecular nuclei (DMN) were obtained by using PROMET.[31] The program SCHAKAL 93 was used for the graphical representation of the results.[32]

Acknowledgements

D. B. and F. G. thank the Ministero della Università e della Ricerca Scientifica e Tecnologica (MURST) (Italy) for financial support, D. B., F. G. and M. J. C. acknowledge the Consiglio Nazionale delle Ricerche (Italy) and the Junta Nacional de Investigação Científica e Technológica JNICT (Portugal) for joint financial support and P. E. M. L. thanks the ERASMUS project 'Crystallography' for subsidizing his stay at the University of Bologna and the JNICT for a grant (BD 2527/RM93).

References

1 See, for example, G. R. Dobson and R. K. Sheline, *Inorg. Chem.*, 1963, **2**, 1313; M. Poliakoff and J. J. Turner, *Chem. Commun.*, 1970, 1008; F. A. Cotton and D. L. Hunter, *Inorg. Chim. Acta*, 1974, **II**, L9; J. Knight and M. J. Mays, *Chem. Commun.*, 1970, 1006; C. G. Benson, G. J. Long, J. W. Kolis and D. F. Shivers, *J. Am. Chem. Soc.*, 1985, **107**, 5297; N. Binsted, J. Evans, G. N. Greaves and R. J. Prince, *J. Chem. Soc., Chem. Commun.*, 1987, 1330.

2 B. F. G. Johnson (Editor), *Transition Metal Clusters*, Wiley, New York, 1980, and refs. therein; R. Desirato, jun., and G. R. Dobson, *J. Chem. Educ.*, 1982, **59**, 752.

3 C. H. Wei and L. F. Dahl, *J. Am. Chem. Soc.*, 1969, **91**, 1351; F. A. Cotton and J. M. Troup, *J. Am. Chem. Soc.*, 1974, **96**, 4155.

4 D. Braga, F. Grepioni, L. J. Farrugia and B. F. G. Johnson, *J. Chem. Soc., Dalton Trans.*, 1994, 2911.

5 (*a*) B. E. R. Schilling and R. Hoffmann, *J. Am. Chem. Soc.*, 1979, **101**, 3456; (*b*) J. Li and K. Jug, *Inorg. Chim. Acta*, 1992, **196**, 89; (*c*) E. J. Baerends and A. Rosa, *New J. Chem.*, 1991, **15**, 815; (*d*) D. G. Evans, *J. Chem. Soc., Chem. Commun.*, 1983, 675; (*e*) B. Delley, M. C. Manning, D. E. Ellis, J. Berkowitz and W. C. Trogler, *Inorg. Chem.*, 1982, **21**, 2247; (*f*) J. W. Lauher, *J. Am. Chem. Soc.*, 1986, **108**, 1521; (*g*) D. Braga, A. Rodger and B. F. G. Johnson, *Inorg. Chim. Acta*, 1990, **174**, 185; (*h*) C. Mealli, in *The Synergy between Dynamics and Reactivity at Clusters and Surfaces*, ed. L. J. Farrugia, in the press; (*i*) A. Sironi, *Inorg. Chem.*, 1992, **31**, 299.

6 P. T. Chesky and M. B. Hall, *Inorg. Chem.*, 1983, **22**, 2998; R. D. Barreto, T. P. Fehlner, L.-Y. Hsu and S. G. Shore, *Inorg. Chem.*, 1986, **25**, 3572; M. A. Gallop, M. P. Gomez-Sal, C. E. Housecroft, B. F. G. Johnson, J. Lewis, S. M. Owen, P. R. Raithby and A. H. Wright, *J. Am. Chem. Soc.*, 1992, **114**, 2502; J.-F. Halet, J.-Y. Saillard, R. Lissillour, M. J. McGlinchey and G. Jaouen, *Inorg. Chem.*, 1985, **24**, 218; G. L. Griewe and M. B. Hall, *Inorg. Chem.*, 1988, **27**, 2250; F. A. Cotton and X. Feng, *Inorg. Chem.*, 1991, **30**, 3666; J. F. Riehl, N. Koga and K. Morokuma, *Organometallics*, 1993, **12**, 4788; R. L. DeKock, K. S. Wong and T. P. Fehlner, *Inorg. Chem.*, 1982, **21**, 3203; C. Mealli, *J. Am. Chem. Soc.*, 1985, **107**, 2245; A. R. Pinhas, T. A. Albright, P. Hofmann and R. Hoffmann, *Helv. Chim. Acta*, 1980, **63**, 29.

7 S. Aime, M. Botta, R. Gobetto and D. Osella, *J. Chem. Soc., Dalton Trans.*, 1988, 791; S. Aime, M. Botta, O. Gambino, R. Gobetto and D. Osella, *J. Chem. Soc., Dalton Trans.*, 1989, 1277; A. Foster, B. F. G. Johnson, J. Lewis, T. W. Matheson, B. H. Robinson and W. G. Jackson, *J. Chem. Soc., Chem. Commun.*, 1974, 1042; R. E. Benfield, P. D. Gavens, B. F. G. Johnson, M. J. Mays, S. Aime, L. Milone and D. Osella, *J. Chem. Soc., Dalton Trans.*, 1981, 1535; D. H. Farrar and J. A. Lunniss, *J. Chem. Soc., Dalton Trans.*, 1987, 1249.

8 M. R. Churchill, F. J. Hollander and J. P. Hutchinson, *Inorg. Chem.*, 1977, **16**, 2655.

9 J. W. Gleeson, and R. W. Vaughan, *J. Chem. Phys.*, 1983, **78**, 5384; H. Dorn, B. E. Hanson and E. Motell, *Inorg. Chim. Acta*, 1981, **54**, L71; B. E. Hanson, E. C. Lisic, J. T. Petty and G. A. Iannacone, *Inorg. Chem.*, 1986, **25**, 4062; T. H. Walter, L. Reven and E. Oldfield, *J. Phys. Chem.*, 1989, **93**, 1320.

10 D. Braga, L. J. Farrugia, F. Grepioni and A. Senior, *J. Chem. Soc., Chem. Commun.*, 1995, 1219.

11 D. Braga, A. W. Bott, C. E. Anson, B. F. G. Johnson and E. A. Marseglia, *J. Chem. Soc., Dalton Trans.*, 1990, 3517.

12 R. Hoffmann, *J. Chem. Phys.*, 1963, **39**, 1397; R. Hoffmann and W. N. Lipscomb, *J. Chem. Phys.*, 1962, **36**, 2179, 3489.

13 A. Gavezzotti, *J. Am. Chem. Soc.*, 1991, **113**, 4622; *Acc. Chem. Res.*, 1994, **27**, 309.

14 (*a*) D. Braga, F. Grepioni, P. Sabatino and A. Gavezzotti, *J. Chem. Soc., Dalton Trans.*, 1992, 1185; (*b*) D. Braga, F. Grepioni and A. G. Orpen, *Organometallics*, 1994, **13**, 3544; (*c*) D. Braga, F. Grepioni, A. G. Orpen and E. Tedesco, *J. Chem. Soc., Dalton Trans.*, 1995, 1215.

15 (*a*) D. Braga, P. J. Dyson, F. Grepioni, B. F. G. Johnson and M. J. Calhorda, *Inorg. Chem.*, 1994, **33**, 3218; (*b*) F. Grepioni, D. Braga, P. Dyson, B. F. G. Johnson, F. M. Sanderson, M. J. Calhorda and L. F. Veiros, *Organometallics*, 1995, **14**, 121; (*c*) D. Braga, F. Grepioni, M. J. Calhorda and L. Veiros, *Organometallics*, 1995, **14**, 1992.

16 C. H. Wei, *Inorg. Chem.*, 1969, **8**, 2384; F. H. Carré, F. A. Cotton and B. A. Frenz, *Inorg. Chem.*, 1976, **15**, 380; P. Corradini, *J. Chem. Phys.*, 1959, **31**, 1676; M. R. Churchill and J. P. Hutchinson, *Inorg. Chem.*, 1978, **17**, 5328; D. Braga, F. Grepioni, J. J. Byrne and M. J. Calhorda, *J. Chem. Soc., Dalton Trans.*, preceding paper.

17 F. A. Cotton, *Inorg. Chem.*, 1966, **5**, 1083; F. A. Cotton and B. E. Hanson, *Rearrangements in Ground and Excited States*, ed. P. De Mayo, Academic Press, New York, 1980, p. 379.
18 A. Sironi, *Inorg. Chem.*, in the press.
19 T. A. Albright, J. K. Burdett and M.-H. Whangbo, *Orbital Interactions in Chemistry*, Wiley, New York, 1985.
20 D. L. Thorn and R. Hoffmann, *Inorg. Chem.*, 1978, **17**, 126; S. Shaik and R. Hoffmann, *J. Am. Chem. Soc.*, 1980, **102**, 1194; E. D. Jemmis, A. R. Pinhas and R. Hoffmann, *J. Am. Chem. Soc.*, 1980, **102**, 2576; D. G. Evans, *J. Chem. Soc., Chem. Commun.*, 1983, 675; R. H. Crabtree and M. Lavin, *Inorg. Chem.*, 1986, **25**, 805; A. A. Low, K. L. Kunze, P. J. MacDougall and M. B. Hall, *Inorg. Chem.*, 1991, **30**, 1079.
21 D. Braga and F. Grepioni, *Acc. Chem. Res.*, 1994, **27**, 51.
22 D. Braga and F. Grepioni, *Organometallics*, 1991, **10**, 1254.
23 A. Gavezzotti and G. Filippini, *Acta Crystallogr., Sect. B*, 1993, **49**, 868.
24 A. Gavezzotti, OPEC, Organic Packing Potential Energy Calculations, University of Milan, 1982; *J. Am. Chem. Soc.*, 1983, **195**, 5220.
25 J. Maddox, *Nature (London)*, 1988, **335**, 201; J. Perlstein, *J. Am. Chem. Soc.*, 1994, **116**, 455; P. Dauber and A. T. Hagler, *Acc. Chem. Res.*, 1980, **13**, 105.
26 J. H. Ammeter, H.-B. Bürgi, J. C. Thibeault and R. Hoffmann, *J. Am. Chem. Soc.*, 1978, **100**, 3686.
27 C. Mealli and D. M. Proserpio, *J. Chem. Educ.*, 1990, **67**, 39.
28 A. Gavezzotti and M. Simonetta, *Chem. Rev.*, 1981, **82**, 1; A. J. Pertsin and A. I. Kitaigorodsky, *The Atom–Atom Potential Method*, Springer, Berlin, 1987.
29 A. Gavezzotti, *Acta Crystallogr., Sect. A*, 1975, **31**, 645.
30 D. E. Williams, PCK 83, A Crystal Molecular Packing Analysis Program, Quantum Chemistry Program Exchange, Indiana University, Bloomington, IN, 1983, no. 481.
31 A. Gavezzotti, PROMET, A Program for the Generation of Possible Crystal Structures from the Molecular Structure of Organic Compounds, Milano, 1992.
32 E. Keller, SCHAKAL 93, Graphical Representation of Molecular Models, University of Freiburg, 1993.

Received 4*th April* 1995; *Paper* 5/02164B